Limits on light WIMPs with a 1 kg-scale germanium detector at 160 eVee physics threshold at the China Jinping Underground Laboratory

Article · January 2018

CITATIONS
11

READS
101

68 authors, including:

Litao Yang
Tsinghua University
73 PUBLICATIONS **795** CITATIONS
SEE PROFILE

Qian Yue
Tsinghua University
350 PUBLICATIONS **7,681** CITATIONS
SEE PROFILE

Liqi Chen
Third Institute of Oceanography China
31 PUBLICATIONS **1,156** CITATIONS
SEE PROFILE

Mehmet Agartioglu
Academia Sinica
45 PUBLICATIONS **478** CITATIONS
SEE PROFILE

Limits on light WIMPs with a 1 kg-scale germanium detector at 160 eVee physics threshold at the China Jinping Underground Laboratory

L.T. Yang,[1,2] H.B. Li,[3,*] Q. Yue,[1,†] K.J. Kang,[1] J.P. Cheng,[1] Y.J. Li,[1] H.T. Wong,[3,*] M. Ağartioğlu,[3,*] H.P. An,[1,2] J.P. Chang,[4] J.H. Chen,[3,*] Y.H. Chen,[5] Z. Deng,[1] Q. Du,[6] H. Gong,[1] L. He,[4] J.W. Hu,[1] Q.D. Hu,[1] H.X. Huang,[7] L.P. Jia,[1] H. Jiang,[1] H. Li,[4] J.M. Li,[1] J. Li,[1] X. Li,[7] X.Q. Li,[8] Y.L. Li,[1] F.K. Lin,[3,*] S.T. Lin,[6] S.K. Liu,[6] Z.Z. Liu,[1] H. Ma,[1,‡] J.L. Ma,[1] H. Pan,[4] J. Ren,[7] X.C. Ruan,[7] B. Sevda,[3,*] V. Sharma,[3,9,*] M.B. Shen,[5] L. Singh,[3,9,*] M.K. Singh,[3,9,*] C.J. Tang,[6] W.Y. Tang,[1] Y. Tian,[1] J.M. Wang,[5] L. Wang,[1] Q. Wang,[1] Y. Wang,[1] S.Y. Wu,[5] Y.C. Wu,[1] H.Y. Xing,[6] Y. Xu,[8] T. Xue,[1] S.W. Yang,[3,*] N. Yi,[1] C.X. Yu,[8] H.J. Yu,[4] J.F. Yue,[5] X.H. Zeng,[5] M. Zeng,[1] Z. Zeng,[1] Y.H. Zhang,[5] M.G. Zhao,[8] W. Zhao,[1] J.F. Zhou,[5] Z.Y. Zhou,[7] J.J. Zhu,[6] and Z.H. Zhu[5]

(CDEX Collaboration)

[1] *Key Laboratory of Particle and Radiation Imaging (Ministry of Education) and Department of Engineering Physics, Tsinghua University, Beijing 100084*
[2] *Department of Physics, Tsinghua University, Beijing 100084*
[3] *Institute of Physics, Academia Sinica, Taipei 11529*
[4] *NUCTECH Company, Beijing 100084*
[5] *YaLong River Hydropower Development Company, Chengdu 610051*
[6] *College of Physical Science and Technology, Sichuan University, Chengdu 610064*
[7] *Department of Nuclear Physics, China Institute of Atomic Energy, Beijing 102413*
[8] *School of Physics, Nankai University, Tianjin 300071*
[9] *Department of Physics, Banaras Hindu University, Varanasi 221005*

(Dated: October 19, 2017)

We report results of a search for light weakly interacting massive particles (WIMPs) dark matter from CDEX-1 experiment at the China Jinping Underground Laboratory (CJPL). Constraints on WIMP-nucleon spin-independent (SI) and spin-dependent (SD) couplings are derived with a physics threshold of 160 eVee, from an exposure of 737.1 kg-days. The SI and SD limits extend the lower reach of light WIMPs to 2 GeV and improve over our earlier bounds at WIMPs mass less than 6 GeV.

PACS numbers: 95.35.+d, 29.40.-n

I. INTRODUCTION

Compelling evidences from astroparticle physics and cosmology indicate that dark matter constitutes about 27% of the energy density of our Universe [1]. WIMPs are the leading candidate for cold dark matter [2] which is one kind of dark matter components.

With excellent energy resolution and low threshold, a kind of *p*-type point contact germanium detector (*p*PCGe) [3, 4] has been used and further developed to search light WIMPs in recent years. Earlier measurements of the phase-I experiment of CDEX collaboration (CDEX-1) [4–6] have provided results on low-mass WIMPs searches with a *p*PCGe of target mass 994 g, and the physics threshold has achieved 475 eVee ("eVee" represents electron equivalent energy). For CDEX, lower energy threshold and lower background level are two main directions of pursuing to get more sensitive results on low mass dark matter searches.

Focused on the lower threshold, a new 1kg-scale *p*PCGe has been designed and customized (named "CDEX-1B" in this report) based on our first prototype detector used in CDEX-1. The point electrode contact was further redesigned to get lower detector capacitance. A junction field-effect transistor (JEFT) with lower noise was selected to be used in an updated pre-amplifier specially designed for CDEX-1B. The supporting structure inside the cryostat had also been modified to further depress background level.

Details of the CDEX-1B experimental setup, data analysis, and the constraints on WIMP-nucleon elastic scattering based on an exposure of 737.1 kg-days at CJPL are discussed in the subsequent sections.

II. EXPERIMENTAL SETUP

The shielding configuration of CDEX-1B is depicted in Fig. 1. The Germanium (Ge) cryostat and NaI(Tl) Anti-Compton detectors are inside the oxygen free high conductivity (OFHC) copper shielding with a thickness of 20 cm, then enclosed by an acrylic box, which was purged by nitrogen gas evaporated from the liquid nitrogen dewar. Other passive shielding includes, from inside to outside, 20 cm of borated polyethylene, 20 cm of lead and 1 m of polyethylene [4]. The detailed information about the passive shielding system was described in Ref. [7].

* Participating as a member of TEXONO Collaboration
† Corresponding author: yueq@mail.tsinghua.edu.cn
‡ Corresponding author: mahao@mail.tsinghua.edu.cn

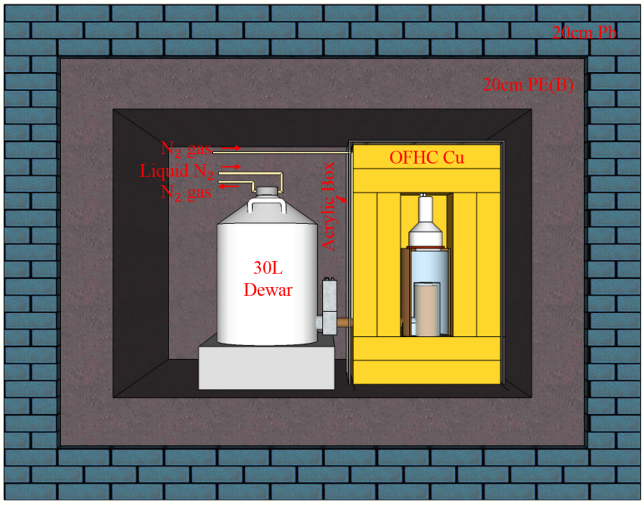

FIG. 1. Schematic diagram of CDEX-1B experimental setup, which includes the Germanium (Ge) detector and NaI(Tl) Anti-Compton detector, as well as the enclosing acrylic box and other passive shielding including the oxygen free high conductivity copper, borated polyethylene and lead. The entire structure is placed inside a 1 m of polyethylene room (PE) described in Ref. [7].

The schematic diagram of the electronics and data acquisition (DAQ) system is shown in Fig. 2. The signals were read out by a pulsed reset preamplifier from the p^+ electrode of the pPCGe and the preamplifier has four identical energy-related outputs. Two of them were distributed into shaping amplifiers with high gain for low energy region (0-12 keV) at different shaping time, 6 μs ($SA_{6\mu s}$) and 12 μs ($SA_{12\mu s}$), respectively. The other two outputs were loaded to timing amplifier (TA) which keep relatively accurate time information. One with high gain for medium energy region (0-20 keV) supplied the charge collection time, the other one with low gain for high energy region (0-1.3 MeV) can be used to analyze the background origin.

Those signals from amplifiers were sampled and recorded by a 100 MHz flash analog-to-digital convertor (FADC). The recording time intervals were 120 μs for each channel. The output of $SA_{6\mu s}$ was fed into the discriminator to supply the trigger of the DAQ system. In addition to that, the discriminator outputs of a random trigger events at 0.05 Hz and the reset inhibit signal also served as triggers and were digitized as well. These random trigger (RT) events will be used to estimate the dead time of the DAQ system and derive the efficiencies of those analysis selection procedures which are uncorrelated with the pulse shape of the signal from Ge detector. The reset inhibit signal recorded the timing of discharging and a veto period of 10 ms was applied after every reset to reject electronic-induced noise. The photomultiplier tube (PMT) outputs from the NaI(Tl) Anti-Compton detector at two different gain factors were also digitized.

The germanium crystal mass of CDEX-1B is 1008 g, almost identical with the crystal used in CDEX-1. The main performance parameters of CDEX-1B are measured and listed in Tab. I, compared with those from CDEX-1. The pedestal RMS achieves 31 eVee, while that for CDEX-1 is 55 eVee. The full width at half maximum (FWHM) of a pulser input is 80 eVee, while that for CDEX-1 is 130 eVee. The FWHM at 10.37 keVee X-rays peak from ^{68,71}Ge is 177±3 eVee. With all these improvements, a physics analysis threshold of 160 eVee at 17% signal selection efficiency is achieved, which is significantly lower than earlier achievement by "CDEX-1".

Starting on March 27th, 2014, the background measurement of CDEX-1B has running for 786.3 days until July 2017, apart from the calibrations by gamma sources, neutron sources, and dead layer measurement performed in August 2014, January 2015 and March 2016, respectively. The dead time ratio of DAQ system kept stable and was <0.1% as measured by RT events.

The optimal area from $SA_{6\mu s}$ channel [6] was chosen to define as the energy (E) for its excellent energy linearity at low energy range. Energy calibration was achieved by the internal cosmogenic X-ray peaks: ^{68}Ge (10.37 and 1.30 keVee), ^{68}Ga (9.66 keVee), ^{65}Zn (8.98 keVee) and the zero-energy was defined by the RT events. The linearity is so good that the deviation is less than 0.4%.

III. DATA ANALYSIS

Due to the extremely small cross section between WIMPs and nucleons, WIMP-nucleon (χ-N) interactions are characterized by being single-site events uncorrelated with other detector components, while having the same pulse shape due to genuine physical processes [8]. A series of data analysis criteria were adopted to select the WIMP-nucleon events, and their corresponding signal efficiencies were measured. The details are discussed as follows:

(1) Anti-Compton Veto (AC): The charge drifts in the Ge detector for a certain amount of time, while the photon in NaI(Tl) Anti-Compton detector is detected without time delay. The time difference between NaI(Tl) Anti-Compton detector and Ge detector can be used to select the coincidence (anti-coincidence) events, which are denoted as $AC^{+(-)}$, respectively. Physical events induced by γ-rays are selected by AC^+ tag and are used to optimize the selection criteria and to calculate the selection efficiencies. The AC^- selection discriminates γ-ray induced background at a signal efficiency of 100%, as measured by RT events.

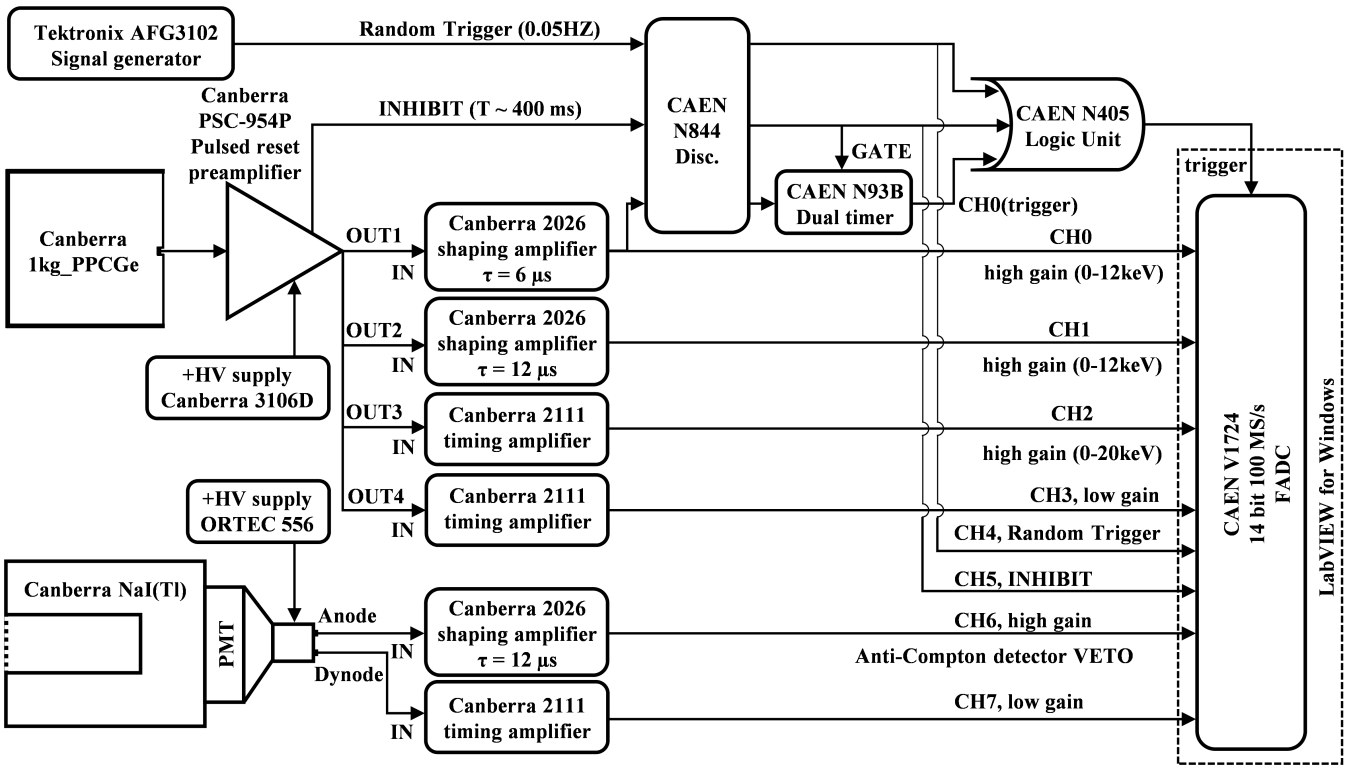

FIG. 2. Schematic diagram of the electronics and the DAQ system of the germanium detector and the NaI(Tl) detector.

TABLE I. The performance parameters of CDEX-1B, compared with the detector used in CDEX-1 [4–6].

Crystal	Pedestal RMS	FWHM of Pulser	Energy at 50% Trigger Efficiency	Physics Analysis Threshold	Combined Signal Efficiency at Threshold
CDEX-1	55 eVee	130 eVee	246 ± 2 eVee	475 eVee	80%
CDEX-1B	31 eVee	80 eVee	126 ± 2 eVee	160 eVee	17%

[a]Full width at half maximum (FWHM).

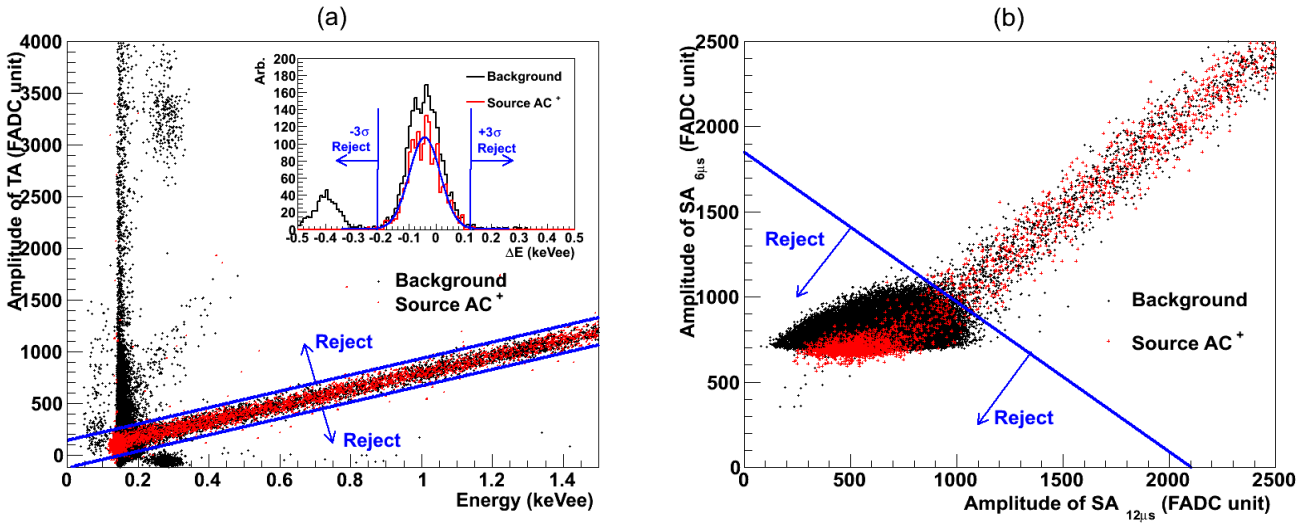

FIG. 3. Two energy-dependent selections near energy threshold based on (a) correlations between the relative amplitude of TA channel (TA_{amp}) and calibrated energy; (b) correlations between the amplitude from $SA_{6\mu s}$ and $SA_{12\mu s}$ (PN).

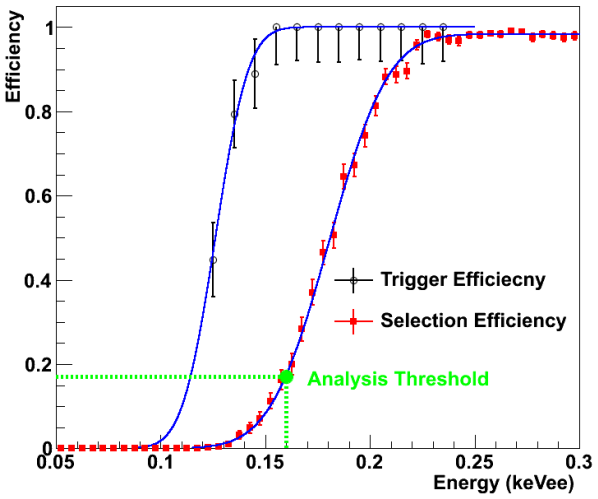

FIG. 4. The combined selection efficiencies and trigger efficiencies derived from the source events in the low energy range are depicted respectively, fit with Error Functions.

(2) Basic Cuts (BC): Signals from reset inhibit of the pre-amplifier or high energy events saturating the timing amplifier can induce abnormal pulses following closely. In addition to a hardware time cut of 10 ms to remove the majority of the reset-induced noises from the reset inhibit signals, the correlations between the TA amplitude (TA_{amp}) and calibrated energy from AC^+ events was used to reject the rest of induced noise, as displayed in Fig. 3 (a). The signal selection efficiency is derived from the survival of AC^+ events from gamma source samples (^{137}Cs, ^{60}Co and ^{241}Am) and ambient background.

Pedestal of $SA_{6\mu s,12\mu s}$ and TA (Ped) cuts were also applied to discriminate those events whose pedestals exhibit anomalous behavior. Apart from using the minima (MIN) and the location of the maxima (t_{MAX}) to remove abnormal events, the correlations between the amplitude from $SA_{6\mu s}$ and $SA_{12\mu s}$ (PN) was used to discriminate physics events from a large amount of noise near threshold, as displayed in Fig. 3 (b). Detailed discussion about these selection cuts can be found in the literature [6, 8].

Selection efficiency of energy-independent cuts (Ped) is derived by the survival of the RT events to be 98.4%, while those for energy-dependent selections (TA_{amp}, MIN, t_{MAX}, PN) are from the survival of AC^+ events from source samples and *in situ* background. Depicted in Fig. 4 is the combined efficiency caused by those BC selections. Trigger efficiency defined as the fraction of the amplitude distribution above the discriminator threshold, was derived with AC^+ events from source samples. The trigger efficiency is displayed in Fig. 4, showing a 50% trigger threshold of 126±2 eVee. In this analysis, the physics analysis threshold is selected to be 160 eVee, which is corresponding to a combined efficiency of 17%.

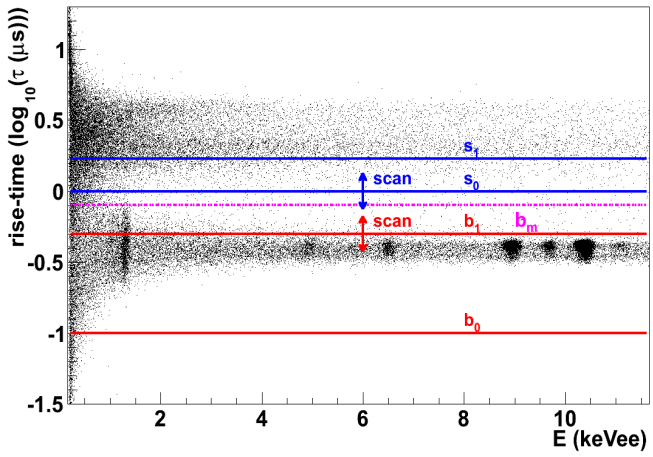

FIG. 5. Rise-time versus energy scatter plot for the WIMP-induced candidate events based on AC^- selection in CDEX-1B data. The solid lines labeled b_0, b_1, s_0, s_1 are related to a relatively pure bulk region [b_0, b_1] and a pure surface region [s_0, s_1], which are used to derived the scaling factors [10]. The dash line labeled b_m is used to calculated the measured bulk count rate B_m roughly, which should be corrected at low energy to get the real count rate B_r. Detailed procedures are described in Ref. [10].

(3) Bulk and Surface event selection (BS): The outer n^+ dead layer of pPCGe is fabricated by lithium diffusion. Events depositing energy in the surface layer will have a partial charge collection with slower rise time (τ) than those in the bulk volume. The charge collection efficiency as a function of the depth of the surface was measured and simulated, showing that the thickness of dead layer for CDEX-1B detector is 0.88±0.12 mm [9]. This gives rise to a fiducial mass of 939 g and data exposure of 737.1 kg-days for this analysis.

The scatter plot of $\log_{10}[\tau]$ versus measured energy E of AC^- events from CDEX-1B is depicted in Fig. 5. The band structure characterizing bulk (B) and surface (S) events is well separated at energy larger than 2 keVee. The K-shell X-rays and L-shell X-rays from internal cosmogenic radioactivity are clearly identified. To get the corrected rates of bulk events (B_r) at low energy region of interest, the Ratio Method has been developed and detailed in previous paper [10]. The solid lines labeled b_0, b_1, s_0, s_1 are related to a relatively pure bulk region [b_0, b_1] and a pure surface region [s_0, s_1], which are used to derived the scaling factors [10]. In order to ensure the consistency between background and those sources used to implement calibration, [s_0, s_1] was chosen to be close to the bulk band. Events with $\tau > s_1$ are removed as very-surface events and will be added back to the surface counts after calibration. The dash line labeled b_m (set as $\tau = 0.8$ μs in this analysis) is used to calculated the measured bulk count rate B_m roughly, which should be corrected at low energy to get the real count rate B_r. Accordingly, the physics events are categorized by "$AC^{-(+)}\otimes B_{r(m)}$" and "$AC^{-(+)}\otimes S_{r(m)}$", where the superscript $-(+)$ denotes anti-coincidence(coincidence)

with the Ge signals, and $B_r(m)$ or $S_r(m)$ denotes the bulk or surface count rates after(before) the BS correction.

The validity of this analysis requires calibration source data with consistent pulse shapes. These conditions have been checked and confirmed to be valid for sources (AC^-, AC^+, ^{137}Cs, ^{60}Co) which give consistent pulse shapes both for the Bulk-samples and the Surface-samples at keV energy. These are adopted as calibration to derive the Bulk (B_r) and Surface (S_r) events from measurements. At near-threshold energy region, resolution effects smear out all intrinsic rise time difference, such that the measured pulse shapes are the same for all sources [10]. The ^{241}Am low-energy γ's are heavily attenuated by the surface thickness such that it is adopted as calibration probability density functions (PDFs) for S-samples only.

The main contributions to the total error of $AC^-\otimes B_r$ at threshold and at a typical high energy bin are summarized in Tab. II. Standard error propagation techniques are used to evaluate the combined uncertainties of B_r and S_r. As discussed in [10], the contribution of systematic uncertainties at energy near threshold mainly comes from the choice of calibration sources and the choice of τ regions.

The measured raw spectra and those at different stages of the analysis are depicted in Fig. 6 (a). Combining the systematic errors and statistical errors, the constructed $AC^-\otimes B_r$ spectrum is depicted in the inset, also the measured $AC^-\otimes B_m$ ($\tau < 0.8$ μs) spectrum. The trigger efficiency and cut efficiency have been considered. The minimum energy is at 160 eVee, matching the first finite efficiency bin of Fig. 4. Several characteristic X-rays peaks from internal cosmogenic radioactive isotopes can be identified clearly, and include ^{68,71}Ge, ^{68}Ga, ^{73,74}As, ^{65}Zn, ^{55}Fe, ^{54}Mn, ^{49}V. As the characteristic X-rays are internal and short-ranged, the detection efficiency is almost 100%. Fig. 6 (b) displays the $AC^+\otimes B_r$ and $AC^+\otimes B_m$ spectra, X-rays peaks from ^{68}Ga (9.66 keVee), ^{65}Zn (8.98 keVee), ^{57,60}Co (7.11 keVee), ^{54}Mn (5.99 keVee) can be identified, clearly. These peaks are produced from the cascade decay corresponding to related cosmogenic radioactive isotopes, and hence a portion of these high energy gammas escape from the Ge detector and are tagged by the NaI(Tl) Anti-Compton detector. This is a non-trivial demonstration of validity of this analysis, since every energy bin is processed independently of the others.

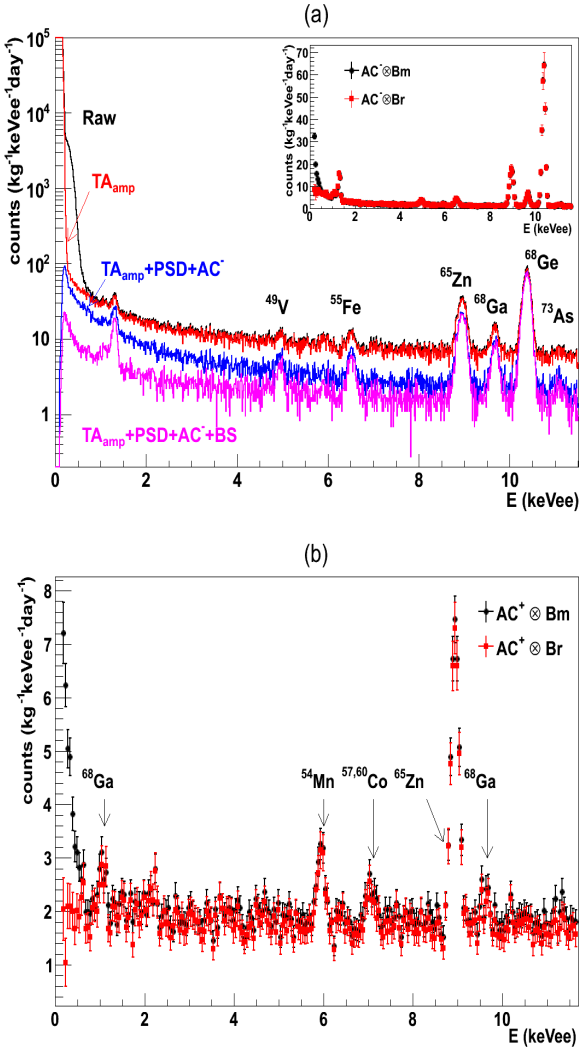

FIG. 6. (a) Measured energy spectra of CDEX-1B, showing the raw spectra and those at the different stages of the analysis, constructed $AC^-\otimes B_r$ spectra and the measured $AC^-\otimes B_m$ ($\tau < 0.8$ μs) spectra are depicted in the inset. (b) AC^+ spectra, some X-rays peaks have also been identified.

IV. RESIDUAL SPECTRUM ANALYSIS

The ratios of the K-shell to L-shell X-ray events based on Ref. [11] are used to predict the intensity of the L-shell X-rays in the lower energy ranges (<1.6 keVee). In addition to the L-shell X-rays contributions, there are residual excess events in the AC^- spectrum at low energy <3 keVee. Several candidate sources were examined but all fail to explain these anomalous events, discussed as follows:

1) Cosmic rays: With a rock overburden of more than 2400 m giving rise to a measured muon flux of 61.7 $y^{-1}m^{-2}$ [12] at CJPL, the contribution from muon can be neglected.

2) Neutrons: Simulation studies and measurements with ^{232}Cf neutron source show neutron-induced events in both AC^- and AC^+ spectra. This excess is not observed in the AC^+ spectra. The thermal neutron flux around the Copper shielding has been measured with a ^{3}He Tube, and the thermal neutron flux is $(2.8\pm1.2)\times10^{-8}$ $cm^{-2}s^{-1}$ [13]. By simulations with Geant4 [14], the contributions from thermal neutron can be also neglected.

TABLE II. The main contributions to the total error of $AC^{-}\otimes B_r$ at threshold and at a typical high energy bin.

Energy Bin	0.16-0.21 keVee	1.96-2.01 keVee
$AC^{-}\otimes B_r$ and Errors	8.38 ± 1.41[stat] ± 2.19[sys]	2.93 ± 0.36[stat] ± 0.17[sys]
($kg^{-1}keV^{-1}day^{-1}$)	$= 8.38 \pm 2.61$	$= 2.93 \pm 0.40$
I) Statistical Uncertainties :	1.41	0.36
II) Systematic Uncertainties :		
(i) Choice of [b_0, b_1], [s_0, s_1]	1.09	0.13
(ii) Choice of sources	1.18	0.05
(iii) Shift of τ by 0.02 ($\log_{10}(\mu s)$)	1.22	0.09
(iv) τ bin-size	0.87	0.03
Combined :	2.19	0.17

3) Tritium: Tritium (^{3}H) will produce a continuous beta energy spectrum with an end point energy of 18.6 keV. The spectrum should be almost flat below 2 keVee and will not contribute to the abnormal rising. From the cosmic ray simulation combined with background data analysis, ^{3}H count rate is 1.81 $kg^{-1}day^{-1}$ at energy range 0-18.6 keVee, far less than the current background count rate of 13.34 $kg^{-1}day^{-1}$.

4) Other possibilities: Extensive cases related to the passivated surface, such as excess ^{210}Pb or ^{210}Po on the tin at the central contact or the signal readout brass bin, the degraded beta emissions from ^{40}K in PTFE, etc., have been carried out to explain those anomalous counts. These depend on the details of material components in the vicinity of the crystal. Ongoing research are being pursued.

V. DARK MATTER CONSTRAINTS

A conservative analysis with only the subtraction of the L/M-shell X-rays was performed. As decpited in Fig. 7 (a), the contributions of the L/M-shell X-rays are derived from K-shell X-rays intensities. The final residual spectrum with L/M-shell X-rays contributions subtracted in the region 0.16-2.5 keVee is shown in Fig. 7 (b), together with the "being excluded" line at $m_\chi = 3$ GeV/c^2 and spin-independent χ-N cross section $\sigma^{SI}_{\chi N} = 2\times10^{-40}$ cm^2 by Binned Poisson method [15], which is applied to this residual spectrum in this analysis. The quenching factor is provided by the TRIM program [16], coupled with a 10% systematic error implied by the spread of the measured data at the recoil energy of 254 eV to 10 keV. A standard WIMP galactic halo assumption [17] and conventional astrophysical models [18] are used, with the local WIMP density of 0.3 GeV/cm^3 and the Maxwellian velocity distribution with $\nu_0 = 220$ km/s, the escape velocity $\nu_{\rm esc} = 544$ km/s. The energy resolution of the detector is derived from the *in situ* cosmogenic peaks.

The derived exclusion plots for spin-independent χ-N coupling (SI) at 90% confidence level is shown in Fig. 8(a), in which several benchmark experiments [6, 19–27] are superimposed. Constrains for spin-dependent χ-neutron (SD) scattering at 90% confidence level is also shown in Fig. 8(b), along with the allowed regions given by DAMA/LIBRA [20] and exclusion limits from CDEX-1 [6, 29], LUX [23], PandaX-II [24], CDMS [26]. These results extend the low reach of light WIMPs to 2 GeV, improve over our earlier bounds on SI for $m_\chi < 6$ GeV [6] and those from the CRESST-II experiment 2016 [27], while achieve the best sensitivity on SD for $m_\chi < 4$ GeV.

VI. SUMMARY AND PROSPECTS

We report results from a 1kg-scale *p*PCGe detector with a physics threshold of 160 eVee at CJPL. By improving electronics and design, the energy threshold and noise are greatly reduced, moving forward to the goal of detecting low mass dark matter. Conservative constraints on WIMP-nucleon spin-independent and spin-dependent elastic scattering are derived based on an exposure of 737.1 kg-days. These results improve over our earlier bounds at $m_\chi < 6$ GeV [6] while extending the low reach of light WIMPs to 2 GeV, and achieve the best sensitivity on SD for $m_\chi < 4$ GeV, which show the effectiveness of reducing the energy threshold.

The high-statistics data reveals anomalous features with the AC^{-} spectra below 3 keVee. Analysis suggests its possible origin to be at the vicinity of the p^+ contact of the Ge-crystal. Such background can be suppressed through radioactivity screen of materials adopted in future detectors. Electronics will be further optimized to target at lower threshold. The potential reach with target sensitivities of 100 eVee threshold at 0.1 kg^{-1} keV^{-1} day^{-1} background level for 10 kg-year exposure is superimposed in Fig. 8.

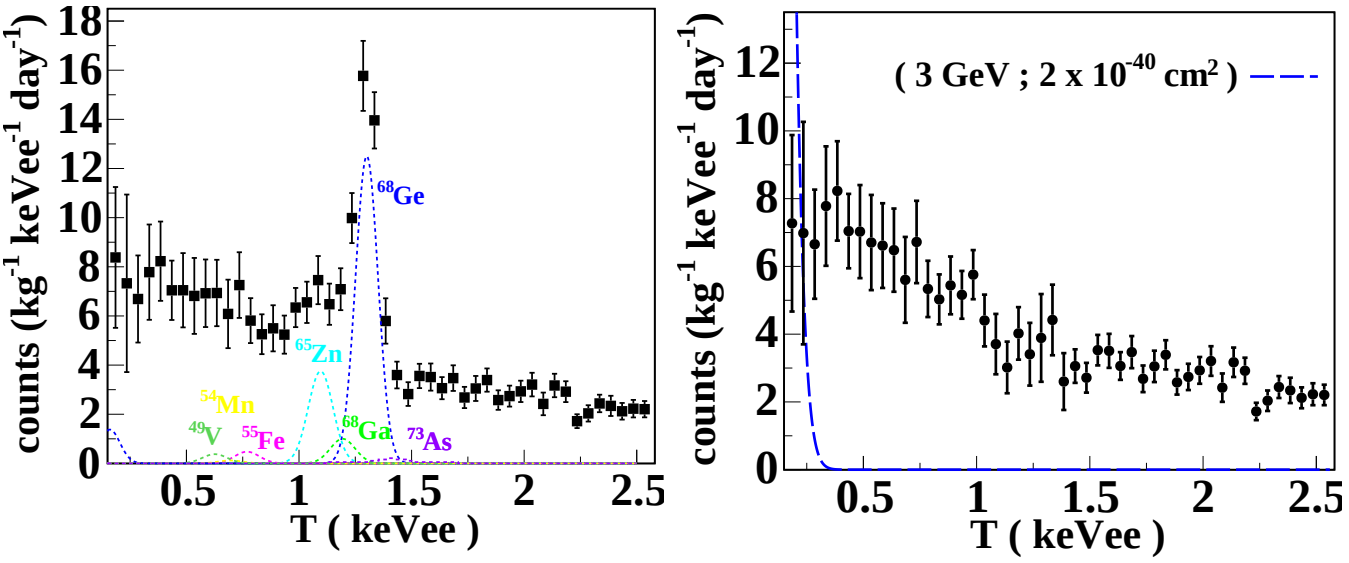

FIG. 7. Left (a): The dashed lines displaying the contributions of the L/M-shell X-rays are derived from K-shell X-rays intensities. Right (b): The residual spectrum with L/M-shell X-rays contributions subtracted, together with the"being excluded" line at $m_\chi = 3$ GeV/c^2 and spin-independent χ-N cross section $\sigma^{SI}_{\chi N} = 2\times10^{-40}$ cm^2 by Binned Poisson method [15].

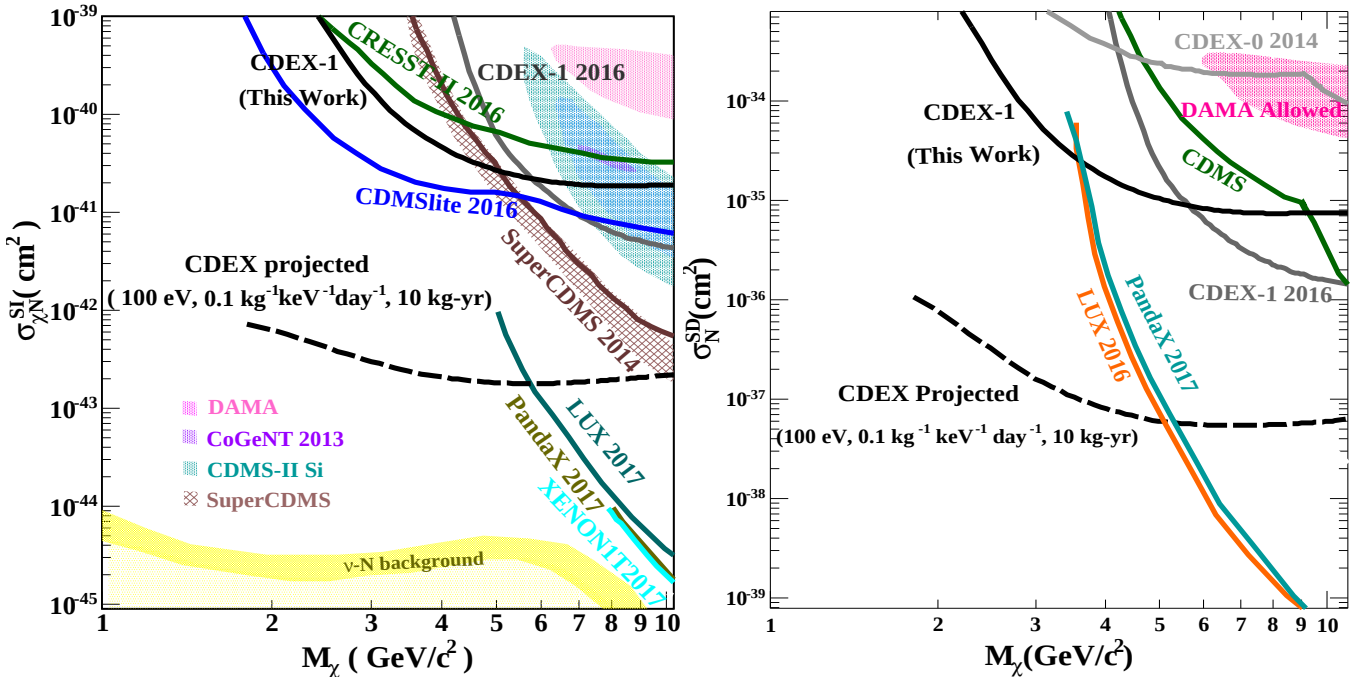

FIG. 8. Left (a): Exclusion plot of spin-independent χ-N coupling at 90% confidence level, superimposed with the results from other benchmark experiments. The CDEX-1 results from this work are depicted in solid black. Allowed regions given by CoGeNT [19], DAMA/LIBRA [20] and CDMS-II (Si) [21] are presented, as well as the exclusion limits from CDEX-1 [6], XENON1T [22], LUX [23], PandaX-II [24], CDMSlite [25], SuperCDMS [26] and CRESST-II [27]. The "Neutrino Floor" due to solar neutrino ν-N scattering is also displayed [28]. Right (b): Exclusion plot of spin-dependent χ-neutron coupling at 90% confidence level, along with the allowed regions given by DAMA/LIBRA [20] and exclusion limits from CDEX-1 [6, 29], LUX [23], PandaX-II [24], CDMS [26]. The potential reach with target sensitivities of 100 eVee threshold at 0.1 kg^{-1} keV^{-1} day^{-1} background level for 10 kg-year exposure are also superimposed both for spin-independent and spin-dependent χN couplings.

ACKNOWLEDGMENTS

This work is supported by the National Key Research and Development Program of China (No. 2017YFA0402200 and 2017YFA0402201) and the National Natural Science Foundation of China (Nos.11175099, 11275107, 11475117, 11475099, 11475092 and 11675088) and the National Basic Research Program of China (973 Program) (2010CB833006) . We thank the support of grants from the Tsinghua University Initiative Scientific Research Program (No.20121088494, 20151080354) and the Academia Sinica Investigator Award 2011-15, contracts 103-2112-M-001-024 and 104-2112-M-001-038-MY3 from the Ministry of Science and Technology of Taiwan.

[1] J. Beringer et al., Phys. Rev. D, **86**, 010001 (2012) and references therein; P. A. R. Ade et al., A&A, **571**, A16 (2014)
[2] C. Kelso, D. Hooper, and M. R. Buckley, Phys. Rev. D, **85**, 043515 (2012) and references therein
[3] P. S. Barbeau et al., J. Cosmol. Astropart. Phys., **09**, 009 (2007)
[4] A. K. Soma et al., Nucl. Instr. Meth. Phys. Res. A, **836**, 67 (2016); W. Zhao et al. (CDEX Collaboration), Phys. Rev. D, **88**, 052004 (2103)
[5] Q. Yue et al. (CDEX Collaboration), Phys. Rev. D, **90**, 091701(R) (2014)
[6] W. Zhao et al. (CDEX Collaboration), Phys. Rev. D, **93**, 092003(R) (2016)
[7] K. J. Kang et al., Front. Phys. **8**, 412 (2013)
[8] Y. C. Wu et al., J. Tsinghua Univ (Sci & Technol), **53**, 1365 (2013)
[9] J. L. Ma et al., Applied Radiation and Isotopes, **127**, 130-136 (2017)
[10] L. T. Yang et al., (2016), arXiv:1611.03357[physics.ins-det]
[11] John N. Bahcall, Phys. Rev., **132**, 362-367 (1963)
[12] Y. C. Wu et al., Chin. Phys. C, **37**, 086001 (2013)
[13] Z. M. Zeng, *Research and Application of Low Background Thermal Neutron Detection Technology*, Ph.D. thesis, Tsinghua University (2017)
[14] Geant4, `http://geant4.web.cern.ch/geant4/`
[15] C. Savage, G. Gelmini, P. Gondolo, and K. Freese, J. Cosmol. Astropart. Phys., **04**, 010 (2009)
[16] J. F. Ziegler, Nucl. Instrum. Methods Phys. Res., Sect. B, **219**, 1027-1036 (2004); S. T. Lin et al. (TEXONO Collaboration), Phys. Rev. D, **79**, 061101 (2009)
[17] F. Donato, N. Fornengo, and S. Scopel, Astropart. Phys., **9**, 247 (1998)
[18] C. E. Aalseth et al. (CoGeNT Collaboration), Phys. Rev. D, **88**, 012002 (2013)
[19] C. E. Aalseth et al., Phys. Rev. D **88**, 012002 (2013)
[20] P. Belli et al., Phys. Rev. D, **84**, 055014 (2011)
[21] R. Agnese et al., Phys. Rev. Lett., **111**, 251301 (2013)
[22] E. Aprile et al. (XENON Collaboration), (2017), arXiv:1705.06655[astro-ph.CO]
[23] D. S. Akerib et al. (LUX Collaboration), Phys. Rev. Lett. **118**, 021303 (2017)
[24] X. Y. Cui et al. (PandaX-II Collaboration), (2017), arXiv:1708.06917[astro-ph.CO]
[25] R. Agnese et al. (SuperCDMS Collaboration), Phys. Rev. Lett., **116**, 071301 (2016)
[26] R. Agnese et al., Phys. Rev. Lett., **112**, 241302 (2014)
[27] G. Angloher et al., The European Physical Journal C, **76**, 25 (2016)
[28] J. Billard et al., Phys. Rev. D, **89**, 023524 (2014)
[29] S. K. Liu et al. (CDEX Collaboration), Phys. Rev. D, **90**, 032003 (2014)